Molecular Frame Image Restoration and Partial Wave Analysis of Photoionization Dynamics of NO by Time-Energy Mapping of Photoelectron Angular Distribution

Ying Tang,* Yoshi-Ichi Suzuki, Takuya Horio, and Toshinori Suzuki†

Chemical Dynamics Laboratory, RIKEN Advanced Science Institute, Wako 351-0198, Japan Department of Chemistry Graduate School of Science, Kyoto University, Kyoto 606-8502, Japan CREST, Japan Science and Technology Agency, Chiyoda-ku, Tokyo 102-0075, Japan

(Received 30 October 2009; published 17 February 2010)

The benchmark system of molecular photoionization dynamics, the $(1 + 1')$ two-photon ionization of NO via the A state, is investigated using the time-energy mapping of the photoelectron angular distribution in a laboratory frame. The molecular frame photoelectron angular distribution and partial wave composition are determined from time-energy maps and compared with those obtained by Schwinger variational calculation (SVC) and state-to-state photoelectron spectroscopy. Good agreement is found with SVC. By comparison of the phase shifts of the scattering waves and the quantum defects of the Rydberg states, the l hybridization of p waves is identified.

DOI: 10.1103/PhysRevLett.104.073002 PACS numbers: 33.60.+q, 33.80.Rv, 82.53.Kp

Molecules are randomly oriented in gases and liquids, and their rotation and liberation persist owing to quantum mechanics. One experimental challenge is to remove directional averaging in physical measurements and ''watch'' electronic structures and dynamics in a molecular frame (MF). Although there have been technical advances in the alignment and orientation of molecules using nonresonant electromagnetic fields [1–3], the axis distribution thus created is still too broad to ignore and often ill characterized to deconvolute from laboratory frame (LF) data.

Resonant photoexcitation creates only a weak axis alignment: one-photon excitation aligns the transition dipole moments within 90° (FWHM) in a LF. However, the created alignment is precise. Taking this advantage, we demonstrate here the restoration of MF photoelectron angular distribution (MFPAD) [4] and a partial wave analysis for the benchmark system of molecular photoionization (PI) dynamics, namely, the $(1 + 1')$ PI of nitric oxide (NO) via the A state [5–9]. Our key strategy is the time-energy (t-E) mapping of LF photoelectron angular distribution (LFPAD) developed in this Letter.

A linearly polarized UV pulse (250 fs, 226.22 nm, 1 kHz) excites NO in a supersonic molecular beam to the vibrational ground level in the $A(^2\Sigma^+)$ state. The rotational temperature of NO in the beam was approximately 3 K, which leads to the population mostly in the lowest rovibronic state ($X^2\Pi_{1/2}$, $v'' = 0$, $J'' = 0.5$). The axes of A-state molecules are perpendicular to the polarization direction of the pump pulse at $t = 0$, while their direction varies with time. The time-dependent molecular axis distribution in LF is expressed as $P(t, \Theta) = (4\pi)^{-1} \times [1 + A(t)P_2(\cos\Theta)]$, $-1 \le A(t) \le 2$, where Θ is the angle between the molecular axis and the polarization direction of the pump pulse, and $P_2(x)$ is the second-order Legendre polynomial. $A(t)$ is accurately calculated from the state multipoles ρ_{KQ} of a coherently excited ensemble of molecules as $A(t) = A_{20}(t)/A_{00}(t)$ with

$$A_{KQ}(t) = \sum_{N_1'J_1'} \sum_{N_2'J_2'} \rho_{KQ}(N_1', J_1', N_2', J_2') \tilde{K} \tilde{N}_1' \tilde{N}_2' \begin{pmatrix} N_2' & K & N_1' \\ 0 & 0 & 0 \end{pmatrix} \times e^{i(E_{N_2'J_2'} - E_{N_1'J_1'})t/\hbar}, \quad (1)$$

in which N_1' and N_2' are the total angular momentum quantum numbers exclusive of electronic and nuclear spin in the A state, J_1' and J_2' are the total angular momentum quantum numbers including electronic spin, $E_{N'J'}$ are rotational energies, and $\tilde{N} = \sqrt{2N + 1}$. The state multipoles are predicted from molecular constants, rotational temperature, and the temporal shape of the pump pulse on the basis of the first-order perturbation theory. A time-delayed linearly polarized probe pulse (100 fs, 323–242.5 nm) ionizes NO from the A state to the $X(^1\Sigma^+)$ state of NO^+, creating an expanding cloud of photoelectrons liberated from molecules. This electron cloud is projected onto a high-performance two-dimensional (2D) position-sensitive detector [10], and the 3D distribution is reconstructed using computer tomography [11]. As we observe the PI process without a vibrational quantum change ($\Delta v = 0$), photoelectron kinetic energy (PKE) varies from 0.05 to 1.33 eV with changing probe laser wavelength [Fig. 1(a)].

LFPAD in two-color two-photon ionization with a parallel polarization of the lasers is expressed as

$$I(t, E, \theta) = \frac{\sigma(t, E)}{4\pi}[1 + \beta_2(t, E)P_2(\cos\theta) + \beta_4(t, E)P_4(\cos\theta)], \quad (2)$$

where t is the pump-probe delay, E is PKE, and θ is the angle between the electron momentum and the polarization direction of the laser. We confirmed that the total electron counts in each photoelectron image measurement exceed 10^7 for photoelectron anisotropy parameters, β_2 and β_4, to converge to their true values within an accuracy of 0.01.

 © 2010 The American Physical Society

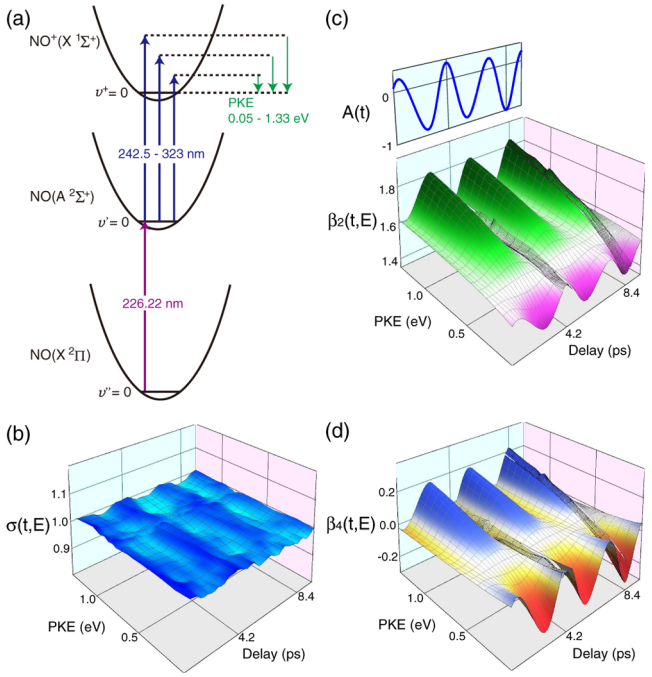

FIG. 1 (color online). (a) The excitation scheme from NO ($X^2\Pi_{1/2}$, $v'' = 0$) to $NO^+(^1\Sigma^+, v^+ = 0)$ via the A ($^2\Sigma^+$, $v' = 0$) state. (b), (c), and (d) Axis alignment factor $A(t)$ and time-energy maps of photoelectron intensity and anisotropy parameters measured as functions of photoelectron kinetic energy and pump-probe time delay. $\sigma(t, E)$ data represent the normalized values at each PKE. The anisotropy parameters were measured at approximately the half (4.2 ps) and full (8.4 ps) revival times with a time window of 0.6 ps, whose regions are identified in the figure as disconnected areas of the surfaces. Photoionization dynamics was analyzed only with these experimental values; the anisotropy parameters at different times in this figure were interpolated to clarify their time dependences.

The actual fitting errors for β_2 and β_4 were both <0.014, and the day-to-day errors were less than 0.008. However, another source of error was the direction of laser beam propagation, as described elsewhere [10]. Therefore the overall accuracies of β deteriorated slightly to <0.03.

$\sigma(t, E)$ and $\beta_L(t, E)$ are expressed by $A_{KQ}(t)$ and the state multipoles of probe light ($\rho^{\gamma}_{k_\gamma 0}$) as [12]

$$\sigma(t,E)\beta_L(t,E) = \sum_{K,k_\gamma=0,2} (-1)^L \tilde{L} \begin{pmatrix} K & L & k_\gamma \\ 0 & 0 & 0 \end{pmatrix} \times \rho^{\gamma}_{k_\gamma 0} A_{K0}(t) b_{KLk_\gamma}(E), \quad (3)$$

where $\rho^{\gamma}_{k_\gamma 0}$ are $1/\sqrt{3}$ and $-\sqrt{2/3}$ for $k_\gamma = 0$ and 2, respectively, for linearly polarized probe light. $\beta_0(t, E) \equiv 1$. Figures 1(b)–1(d) show $\sigma(t, E)$, $\beta_2(t, E)$, and $\beta_4(t, E)$ measured as functions of time and PKE. Because these quantities are approximately proportional to $A(t)$, we focused our measurements of $\beta_2(t, E)$ and $\beta_4(t, E)$ on the half (4.2 ps) and full (8.4 ps) rotational revival times when $A(t)$ takes its maximum and minimum, respectively. β_2 and β_4 in the intermediate time range, shown in Fig. 1, were interpolated to demonstrate their time dependences; they were not used in the analysis. On the other hand, the presented $\sigma(t, E)$ data are all experimental values with normalization at each PKE by setting $\sigma(t, E) = 1$ at $t = 0.9$ ps [when $A(t) = 0$].

In our analysis, we first determine the asymptotic form of an electron scattering wave function from $\sigma(t, E)$, $\beta_2(t, E)$, $\beta_4(t, E)$, and $A(t)$. Then, MFPAD is obtained from the wave function. The wave function of a photoelectron, in this case, is expressed as a superposition of l-indexed partial waves with $0 \le l \le 3$ and $\lambda = 0$ or 1 [5–7]. Therefore, seven partial waves are involved. However, since the absolute PI cross section and the overall phase of the wave function are not relevant in this study, six relative amplitudes and six relative phases are sufficient for describing MFPADs. The electron scattering wave function is characterized by the amplitudes and phases of the partial waves. The amplitude of each wave is determined by the magnitude of bound-free transition dipole moments, $r_{l\lambda}$. The scattering phase is generally divided into the dynamical phase shift $\chi_{l\lambda}$ and the Coulomb phase shift $\eta_l(E)$. The former can be approximated to be energy independent in the narrow energy range studied in this Letter, whereas the latter is analytically known. Dipoles and dynamical phase shifts are included in b_{KLk_γ} in Eq. (3) and can be determined by the nonlinear regression (NLR) of experimental t-E maps. Using S-matrix normalized scattering wave functions, $b_{KLk_\gamma}(E)$ are written as

$$b_{KLk_\gamma}(E) = \sum_{ll'\lambda\lambda'\Lambda} (-1)^{l+\lambda+\lambda'+K} \sqrt{3}\tilde{l}\tilde{l}'\tilde{L}\tilde{k}_\gamma \begin{pmatrix} l & l' & L \\ 0 & 0 & 0 \end{pmatrix} \times \begin{pmatrix} l & l' & L \\ \lambda & -\lambda' & \Lambda \end{pmatrix} \begin{pmatrix} 1 & 1 & L \\ -\lambda & \lambda' & -\Lambda \end{pmatrix} \times \begin{pmatrix} L & K & k_\gamma \\ \Lambda & 0 & -\Lambda \end{pmatrix} r_{l\lambda} r_{l'\lambda'} i^{l'-l} \times e^{i[\pi(\chi_{l\lambda}-\chi_{l'\lambda'})+\eta_l(E)-\eta_{l'}(E)]}, \quad (4)$$

where l and λ are the orbital angular momentum and its projection on the molecular axis, respectively.

With the given signal-to-noise ratio of our $\sigma(t, E)$, $\beta_2(t, E)$, and $\beta_4(t, E)$ maps, NLR can determine 11 fitting variables. Thus 6 relative magnitudes ($r_{l\lambda}$) and 5 relative dynamical phases were determined, as presented in Fig. 2(a). The figure also shows a comparison of our result with the values obtained by Schwinger variational calculation (SVC) [5] and state-to-state photoelectron spectroscopy (SSPES) [7]. The remaining relative phase between the even and odd partial waves cannot be determined by t-E mapping and SSPES, and thus we estimated it by continuum multiple scattering $X\alpha$ (CMS-$X\alpha$) calculations: the relative phase between $s\sigma$ and $p\pi$ was calculated to be $(\chi_{s\sigma} - \chi_{p\pi}) = 1.79$ rad, which is in agreement with the estimate (1.85) by SVC [5].

Figures 2(b)–2(d) present 3D graphics of the MFPADs determined by t-E mapping, SVC, and SSPES, respec-

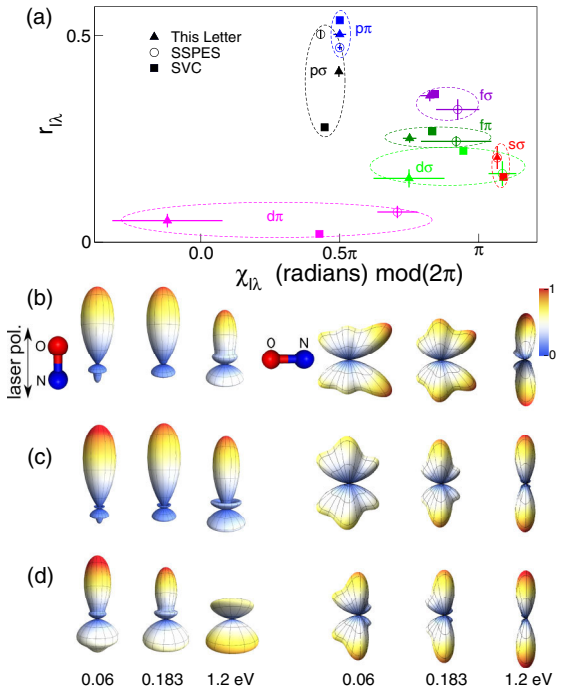

FIG. 2 (color online). (a) The relative amplitudes $r_{l\lambda}$ are plotted with respect to the dynamical phases $\chi_{l\lambda}$ of partial waves obtained through our experiment, SVC [5], and SSPES [7]. The phases are relative values from $\chi_{p\pi}$, which is fixed at $\chi_{p\pi} = 0.5\ \pi$ rad. MFPADs determined by (b) time-energy mapping, (c) SVC, and (d) SSPES.

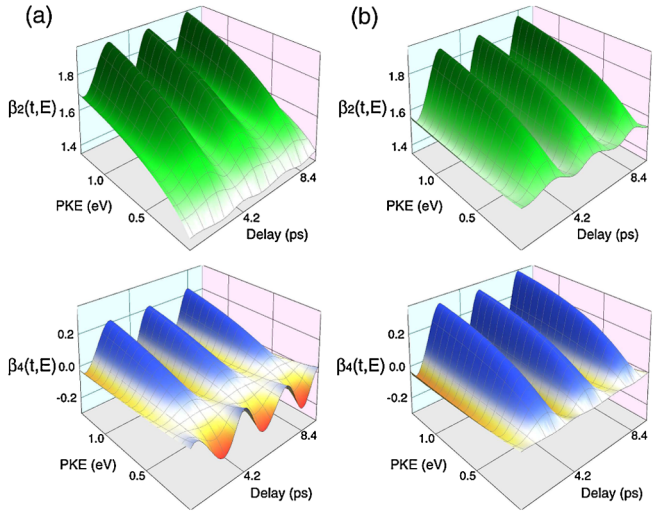

FIG. 3 (color online). Simulated time-energy maps of photoelectron intensity and anisotropy parameters. Simulations based on (a) Schwinger variational calculations [5] and (b) state-to-state photoelectron spectroscopy at $E = 0.183$ eV [7].

tively. As shown in Fig. 2(b), an electron is ejected sharply on the oxygen side at a low PKE in the σ channel, and the distribution gradually grows on the nitrogen side at a high PKE. In the π channel, an electron is ejected at wide angles at a low PKE, creating a butterfly shape, and the distribution becomes narrow along the laser polarization at a high PKE. The asymmetry between the oxygen and nitrogen sides is small in the π channel. The MFPADs of SVC in Fig. 2(c) reproduce these features rather well, except for the π channel at a very low PKE (0.06 eV). Figure 2(d) for SSPES was drawn using the result reported for $E = 0.183$ eV [5] and considering Coulomb phase shifts. A discrepancy is seen between the results of t-E mapping and SSPES in the σ channel, which is understandable for a limited signal-to-noise ratio of SSPES using the time-of-flight method.

Since the MFPADs obtained by t-E mapping and SVC are very similar, we examined whether t-E mapping can discriminate their differences. Figure 3(a) shows the t-E maps calculated from the partial wave compositions reported by SVC. SVC reproduces the anticorrelation of $\beta_2(t, E)$ and $\beta_4(t, E)$ with $A(t)$ at a high PKE and the increasing rotational modulation depth with PKE. However, the calculated modulation is too weak at low PKE, particularly for β_2. The result demonstrates that t-E mapping is sensitive to small differences in MFPAD. Similar plots are shown for SSPES in Fig. 3(b).

Figure 2(a) shows both the magnitude and sign of the phase differences. The interference between the partial waves is generally expressed as $\cos(\phi_b - \phi_a)$, where ϕ is the (overall) phase shift of a scattering wave, and a and b represent different partial waves. Since cosine functions are invariant for the phase reversal to $\phi_b - \phi_a$, PAD generally leaves two possible solutions for the phase relation at a certain energy. One way to determine the true phase is to measure the circular dichroism in PAD [7,13,14] in PI with circularly polarized light. Because the optical phase is transferred to the partial wave and creates the sine function, $\sin(\phi_b - \phi_a)$, the combination of the sine and cosine functions allows for the unique determination of the phase differences [7]. Although, t-E mapping uses only linearly polarized light, $\eta(E)$ changes with PKE, which plays the same role as the ellipticity of light [15]. The t-E maps can be explained only with the unique set of dynamical phases including their signs when analytically known $\eta(E)$ is taken into account. This is an important feature of t-E mapping.

The quantum defect theory (QDT) [8,16,17] relates the scattering state and Rydberg state (RS): the dynamical phase shifts of their wave functions are essentially the same and related to the quantum defect $\delta_{l\lambda}$ of RS as $\chi_{l\lambda} = \pi\delta_{l\lambda}$ [18]. This relation has been experimentally verified for atomic PI [19–22]. However, in a molecular case, this argument requires caution. Although molecular RSs are categorized into s, p, d, etc., from their quantum defects, their actual wave functions may be l hybridized [23], because the orbital angular momentum l is not a good quantum number for a nonspherical system (molecules). In the treatment of PI using a scattering theory, the boundary conditions can be set such that MFPAD is obtained without expressing the hybridization of l-wave explicitly [24]. However, when we compare RSs with scattering

TABLE I. Differences between scattering phase shifts ($\Delta\chi_{l\lambda-p\pi}$) in radians units (mod π). The numbers in parentheses for $\Delta\chi_{l\lambda-p\pi}$ are 1σ uncertainties in our analysis, and those for quantum defects ($\pi\Delta\delta_{l\lambda-p\pi}$) are their variation in the energy range, taken from Ref. [29], in the PKE range studied in this Letter.

$l\lambda$	$p\sigma$	$f\sigma$	$f\pi$
$\Delta\chi_{l\lambda-p\pi}$	−0.006(72)	1.027(79)	0.782(82)
$\pi\Delta\delta_{l\lambda-p\pi}$	−0.267(19)	0.952(35)	0.942(35)

states on the basis of QDT, we must use eigenchannel wave functions for both states in order to correctly account for l hybridization [8,23,25].

The hybridization of Rydberg orbitals was observed experimentally for $s-d$ and weakly for $s-f$ and $d-f$ of NO [26–28], whereas no hybridization was identified for other orbitals. Given that the hybridization of RSs is not precisely known, the prediction of dynamical phase shifts from quantum defects could be inaccurate. On the contrary, any deviation of the observed phase shifts from the prediction will point to the hybridization of l waves. Thus, we compared the phase shift difference $\Delta\chi_{l\lambda-p\pi} \equiv (\chi_{l\lambda} - \chi_{p\pi})$ determined by t-E mapping and those predicted from the difference between the quantum defects of RSs [29], multiplied by π, i.e., $\pi\Delta\delta_{l\lambda-p\pi} \equiv \pi(\delta_{l\lambda} - \delta_{p\pi})$, in Table I. The deviations of the observed $\Delta\chi_{l\lambda-p\pi}$ from the predictions of $\pi\Delta\delta_{l\lambda-p\pi}$ were 0.26 ± 0.07 and -0.16 ± 0.09 rad for $p\sigma - p\pi$ and $f\pi - p\pi$, respectively. The former suggests that p RSs ($p\sigma$ or $p\pi$ or both) are not pure and l hybridized. Consequently, it is concluded that corresponding p scattering waves are also l hybridized.

The observed $\Delta\chi_{f\pi-p\pi}$ can be explained by the hybridization of $p\pi$ and $f\pi$ with off-diagonal elements of -0.11 ± 0.07 in a 2×2 $p-f$ mixing matrix in the π channel [25], by neglecting the small $r_{d\pi}$ shown in Fig. 2(a). The value is 1 order of magnitude larger than that predicted by *ab initio* QDT within frozen-core approximation, i.e., −0.01 [30]. On the other hand, the *ab initio* QDT [30] predicted relatively large off-diagonal elements of $s-p$ and $p-d$ hybridizations in the σ channel, i.e., 0.03 and 0.09, respectively. The experimentally observed relative phases in Table I are consistent with the theory [30] if the difference between $\Delta\chi_{p\sigma-p\pi}$ and $\pi\Delta\delta_{p\sigma-p\pi}$ arises mainly from $s-p-d$ hybridization in the σ channel.

In conclusion, t-E mapping enables the complete determination of PI dynamics with femtosecond time resolution without the need for rotational state resolution. It is important to note that t-E mapping will enable the elucidation of the PI dynamics of large molecules, even if they have rather short excited-state lifetimes.

We would like to thank Professor V. McKoy, Professor C. Jungen, and Professor R. Lucchese for fruitful discussions.

*Present address: Wuhan Institute of Physics and Mathematics, Chinese Academy of Sciences, Wuhan, People's Republic of China.
†t-suzuki@riken.jp

[1] P. R. Brooks, Science **193**, 11 (1976).
[2] B. Friedrich and D. R. Herschbach, Nature (London) **353**, 412 (1991).
[3] T. Seideman, J. Chem. Phys. **103**, 7887 (1995).
[4] D. Dill, J. Chem. Phys. **65**, 1130 (1976).
[5] H. Rudolph and V. McKoy, J. Chem. Phys. **91**, 2235 (1989).
[6] S. W. Allendorf, D. J. Leahy, D. C. Jacobs, and R. N. Zare, J. Chem. Phys. **91**, 2216 (1989).
[7] D. J. Leahy, K. L. Reid, H. Park, and R. N. Zare, J. Chem. Phys. **97**, 4948 (1992).
[8] H. Park and R. N. Zare, J. Chem. Phys. **104**, 4554 (1996).
[9] H. Park and R. N. Zare, J. Chem. Phys. **104**, 4568 (1996).
[10] T. Horio and T. Suzuki, Rev. Sci. Instrum. **80**, 013706 (2009).
[11] T. Suzuki, Annu. Rev. Phys. Chem. **57**, 555 (2006).
[12] Y.-I. Suzuki and T. Suzuki, Mol. Phys. **105**, 1675 (2007).
[13] R. L. Dubs, S. N. Dixit, and V. McKoy, Phys. Rev. Lett. **54**, 1249 (1985).
[14] J. R. Appling, M. G. White, T. M. Orlando, and S. L. Anderson, J. Chem. Phys. **85**, 6803 (1986).
[15] V. Schmidt, *Electron Spectrometry of Atoms Using Synchrotron Radiation* (Cambridge University Press, Cambridge, 1997), p. 202.
[16] U. Fano, Phys. Rev. A **2**, 353 (1970).
[17] *Molecular Applications of Quantum Defect Theory*, edited by C. Jungen (Inst. of Physics Pub., Inc., Bristol, U.K., 1996).
[18] M. J. Seaton, Rep. Prog. Phys. **46**, 167 (1983).
[19] H. Kaminski, J. Kessler, and K. J. Kollath, Phys. Rev. Lett. **45**, 1161 (1980).
[20] L. H. Haber, B. Doughty, and S. R. Leone, Phys. Rev. A **79**, 031401(R) (2009).
[21] J. C. Hansen, J. A. Duncanson, R.-L. Chien, and R. S. Berry, Phys. Rev. A **21**, 222 (1980).
[22] Z.-M. Wang and D. S. Elliott, Phys. Rev. A **62**, 053404 (2000).
[23] C. H. Greene and C. Jungen, Adv. At. Mol. Phys. **21**, 51 (1985).
[24] D. Dill and J. L. Dehmer, J. Chem. Phys. **61**, 692 (1974).
[25] Using QDT, the relations for quantum defects ($\delta_{\alpha\lambda}$) are obtained as $\pi\delta_{\alpha\lambda} = \arg[\sum_l U^{\lambda}_{l\alpha} r_{l\lambda} \exp(i\chi_{l\lambda})]$, for either the σ or π channel, where $\{U^{\lambda}_{l\alpha}\}$ are mixing matrices that are real and unitary.
[26] S. Fredin, D. Gauyacq, M. Horani, C. Jungen, G. Lefevre, and F. Masnou-Seeuws, Mol. Phys. **60**, 825 (1987).
[27] E. Miescher, Can. J. Phys. **54**, 2074 (1976).
[28] S. Pratt, C. Jungen, and E. Miescher, J. Chem. Phys. **90**, 5971 (1989).
[29] E. Miescher and K. P. Huber, *International Review of Science, Physical Chemistry (2)* (Butterworths, London, 1976), Vol. 3, p. 37.
[30] R. Guérout, M. Jungen, and C. Jungen, J. Phys. B **37**, 3057 (2004).